Deformation mechanisms of zirconium alloys after irradiation studied by dislocation dynamics simulations and in situ straining experiments in TEM

Fabien Onimus, Laurent Dupuy, Marine Gaumé, Wassim Kassem, Frederic Mompiou

Symposium: 19th International Symposium on Zirconium in the Nuclear Industry

Paper Title:

Deformation mechanisms of zirconium alloys after irradiation studied by dislocation dynamics simulations and *in situ* straining experiments in TEM

Authors: F. Onimus[1], L. Dupuy[1], M. Gaumé[1], W. Kassem[1], F. Mompiou[2]

[1] DEN, Section for Applied Metallurgy Research, CEA Saclay, Université Paris-Saclay, 91191 Gif-sur-Yvette, Cedex, France

[2]CEMES CNRS and Université de Toulouse, 29 rue Jeanne Marvig, 31055 Toulouse Cedex 4, France

** corresponding author : fabien.onimus@cea.fr*

Abstract: (300 words)

Zirconium alloys, used in the nuclear industry, are subjected to neutron irradiation that affects their mechanical properties. At the microscopic scale, neutron irradiation creates small dislocation loops that act as obstacles against dislocation glide explaining the irradiation hardening. Transmission Electron Microscopy observations performed after post-irradiation mechanical tests have shown that loops are swept out by gliding dislocations creating thin zones free of defects. Observations have proven that slip occurs preferably in the basal plane, a puzzling fact as dislocations mainly glide in the prismatic plane in unirradiated conditions.

In order to understand this phenomenon, discrete Dislocation Dynamics (DD) simulations, on complex configurations, have been performed. The input parameters of this code have been adjusted on MD simulations. Then interactions between loops and mixed dislocations gliding either in the prismatic or basal plane have been simulated. These simulations show that prismatic glide is always impeded in the mixed-screw direction whereas for basal slip, clearing or a weak interaction occurs in the mixed-screw direction, allowing an easy glide of basal dislocations. Furthermore, all three basal systems can contribute to clearing in the basal plane contrary to prismatic slip. These two reasons explain the easy basal glide and clearing of loops after irradiation.

Moreover, *in-situ* straining experiments inside a TEM have been conducted on ion irradiated recrystallized Zircaloy-4. Several interactions between dislocations and loops have been observed in situ. The DD code has been used to simulate these interactions. A fair agreement is obtained between simulations and experiments, showing the relevance of the DD numerical tool.

1. Introduction

Zirconium alloys are widely used as cladding tubes for the nuclear fuel of Light Water Reactors. During in-reactor operation, these materials undergo radiation damage due to fast neutrons. Moreover, they are subjected to various mechanical loadings leading to irreversible visco-plastic deformation. In order to ensure the integrity of the cladding, various empirical models are used. To improve the predictive capability of the numerical simulations, it is of interest to develop physically based models that take into account the microscopic mechanisms.

At the microscopic scale, fast neutron irradiation leads to the formation of point defects that diffuse and cluster together in the form of small dislocation loops. In zirconium alloys, the most stable point defect clusters are the perfect <a> loops, with a Burgers vector $\underline{b} = 1/3\langle 11\bar{2}0\rangle$, located close to the prismatic habit planes [1, 2]. These loops can be either interstitial or vacancy loops. They appear rapidly after the start of irradiation. They are small, typically 10 nm in diameter, and very numerous, with a typical number density of 10^{22} m^{-3}.

The formation of these irradiation defects has a strong influence on the mechanical behavior of the material. It is well established that the hardening measured after irradiation is directly related to formation of <a> loops. Indeed, these loops act as obstacles against dislocation glide. The hardening is associated with a decrease of the uniform elongation and an early necking, the failure remaining ductile. This is due to a loss of work-hardening capability. These phenomena are related to the formation of <a> loops and to their interaction with gliding dislocations.

In order to understand the underlying mechanisms at the origin of the plastic deformation of irradiated zirconium alloys, several authors [3, 4, 5, 6, 7, 8, 9, 10, 11, 12, 13] have analyzed by Transmission Electron Microscopy (TEM) thin foils taken out of samples tested in hot cell after neutron irradiation. Thin white cleared bands were observed after testing. In these bands, loops have been swept away by gliding dislocations, creating zones where further dislocations can glide freely and thus remain confined in these channels. It was shown in [10, 11, 13] that for transverse tensile and internal pressure tests conducted at 350°C, the channels observed after testing were only basal channels whereas in the same testing conditions, easy prismatic slip was observed in the non-irradiated material.

To obtain a better understanding of the processes leading to the channeling phenomenon some authors have conducted Molecular Dynamics (MD) simulations of elementary interactions between individual dislocation and loop [14, 15, 16]. Serra and Bacon [15] studied the interaction between a small square loop and a dislocation, either edge or screw, gliding in a prismatic plane. Ghavam and Gracie [16] recently studied the interaction between a large elliptical loop and a mixed dislocation gliding in the basal plane. No comparison between the two slip systems is provided by the authors. Following the work done by Serra and Bacon [15], Drouet et al. [17] have studied small square loops interacting with a dislocation, either screw or edge only. For this study, the authors used Dislocation Dynamics (DD) simulations. By

applying this method to dislocations gliding either in the prismatic plane or in the basal plane, the authors have been able to understand the reason for the easier glide in the basal plane. However, because the study was limited to pure screw and pure edge dislocations using small simulation box with periodic boundary conditions, some artifacts remained and the overall picture was not fully clarified.

On the experimental side, Onimus et al. [18] and Drouet et al. [19] have conducted in situ TEM straining experiments to observe, at the nanometer scale and in real time, the interactions between dislocations and loops. They managed to observe interactions between loops and dislocations gliding in the prismatic and pyramidal planes. In particular, the incorporation of a vacancy loop into the gliding dislocation was clearly observed in situ and simulated using DD [19].

In order to overcome previous limitations and provide a better understanding for the reason of the easier basal channeling, a new study, based on multi-scale numerical simulations and experiments at the dislocation scale, has been undertaken and is presented in this article.

2. Tools and Methods

2.1. Experiments

A thin sheet made of recrystallized Zircaloy-4 characterized by equiaxed grains of 6 µm diameter has been used. Small samples have been machined out in the form of dog-bone specimens. The middle of the gauge length of the specimen was electropolished on one side only. Then these specimens have been irradiated at a temperature of 450°C using 600 keV Zr ions. Two doses were reached: 8×10^{17} ions/m^2 and 2.4×10^{18} ions/m^2. After ion irradiation, the irradiated side was protected by a varnish and the other side was electropolished to create a small hole with thin area on its side that can be observed by TEM. The mean loop diameter was 30 nm, the loop number density was 6×10^{20} m^{-3} and they were mainly interstitial loops [20].

These specimens were then installed on a specific TEM sample holder able to apply a strain to the sample while heating. In situ straining experiments were then done, at various temperatures. After recording an interesting sequence, the orientation of the grain was analyzed using electronic diffraction. Two interactions are reported in the last part of the article.

2.2. Numerical simulations

In order to assess, starting from the smallest length scale, the details of the interactions between dislocation and loops, MD simulations have been conducted using the code LAMMPS [21]. Following the work done by Serra and Bacon [15], interactions between dislocation and loops have been computed [22].

Because MD simulations are time consuming and limited to small length scale, other types of numerical simulation tools are required in order to investigate more complex configurations and to go up to larger length scale. This is why a discrete DD code, called NUMODIS [19], has been used. In this model, the dislocations are represented by a set of nodes connected by segments. The nodal forces arise from the core energy of the dislocation and the Peach-Koehler forces, due to the local stress tensor, acting on the segments. The local stress tensor is the result of the superposition of the external applied stress and of the stress fields created by all dislocation segments, including the considered segment, present in the simulation box. The velocity of each node is then deduced from a viscous mobility law of the dislocation segment connecting the nodes, given by Equation 1.

$$v = \frac{\tau b}{B} \qquad (1)$$

In Equation 1, B is the friction coefficient, which depends on the glide system of the segment, τ is the resolved shear stress applied on the considered segment, b is the Burgers vector and v is the segment velocity.

Discrete DD simulation requires the introduction of various material dependent parameters. The elastic constants, the shear modulus (μ) and the Poisson's ratio (ν), assuming isotropic elasticity, the friction coefficients B for the various slip systems and also two parameters, a_0 and E^0_{core}, needed to describe the energy per unit length of a dislocation. The elastic energy of a dislocation segment, which is related to the stress field created by the dislocation, is described by the non-singular continuum isotropic elasticity theory of dislocations developed by Cai et al. [23]. In this theory, a parameter a_0, related to the spread of the dislocation core, is introduced. In addition to the elastic energy, the energy of the core of the dislocation is taken into account in the modeling. It is orientation dependent, edge or screw, as for the elastic energy, and can then be expressed as Equation 2.

$$E_{core}(\varphi) = \frac{1-\nu\, cos(\varphi)}{1-\nu} E^0_{core} \qquad (2)$$

In Equation 2, φ is the angle between the Burgers vector and the dislocation segment and E^0_{core} is the core energy of a screw dislocation.

A specific method, described in [22] has been developed to adjust these parameters on MD simulations. From the anisotropic elastic moduli (C_{ij}) of Zr computed at 300K the isotropic elastic parameters are deduced using the procedure described by Scattergood and Bacon [24]. The shear modulus is found equal to 36.3 GPa and Poisson's ratio is found respectively for the prismatic plane equal to 0.223 and 0.365 for the basal plane. The parameters obtained, after adjustment on MD simulations, for the parameters describing the energy per unit length of a dislocation are a_0= 3.3 Å and E^0_{core}= 0.137 eV/Å. The values obtained by MD simulation for the friction coefficients for the prismatic B_P and basal B_B slip are B_P=2.96×10^{-5} Pa.s and B_B=4.56×10^{-5} Pa.s. Furthermore, it has been found that there is an additional dragging force on the constricted nodes on a jogged dislocation, at the intersection of the prismatic and basal

planes. This phenomenon was already observed by Rodney et al. [25] for nickel. In order to account for this additional friction, a simple model was proposed where a specific friction is attributed to these constricted nodes (p expressed in Pa.s.m) and is found to be equal to p =1.72×10^{-13} Pa.s.m. This value has also been introduced into the DD simulations.

Then, as a second step, the MD simulations of interactions between one dislocation and one loop done by Serra and Bacon [15] have been reproduced and are shown in [22], using precisely the same geometrical configurations and loading conditions. Qualitatively and quantitatively, the mechanisms observed are the same as the one described in [15].

It must be pointed out that due to the computational limitations of MD simulations, the box used in [15] is very small and that periodic boundary conditions and the choice to simulate only pure screw and pure edge dislocations induce very symmetrical configurations. This is especially true when the interaction of a screw dislocation interacting with a loop is simulated. Indeed, in that case a helical turn is formed, expanding along the line of the screw dislocation. Because of the too small simulation box and the periodic boundary conditions, the segments of the dislocation, gliding originally in the prismatic plane, disappear. Only remains a segment in the basal plane. To overcome the helical turn, a new segment, gliding in the prismatic plane, nucleates in the middle of the remaining basal segment. For less symmetrical configurations, the segments gliding in the prismatic plane do not disappear and this mechanism is thus not needed. From this analysis, it appears that it is very important to simulate less symmetrical configurations.

Taking advantage of the adjustment and validation of the DD code on MD simulations, more complex configurations than pure screw or pure edge dislocations, have been studied. A dislocation with a mixed character, resulting from the activation of a Frank-Read source has been introduced into a simulation box. It consists in a thin 40 nm box in the z direction, parallel to the glide plane normal, either $(10\bar{1}0)$ or (0001). The length in the two other directions (x and y) is equal to 6 µm. Impenetrable surfaces are used. These surfaces represent grain boundaries. The initial Frank-Read source, screw or edge, of length equal to 150 nm is located in the middle of the box (

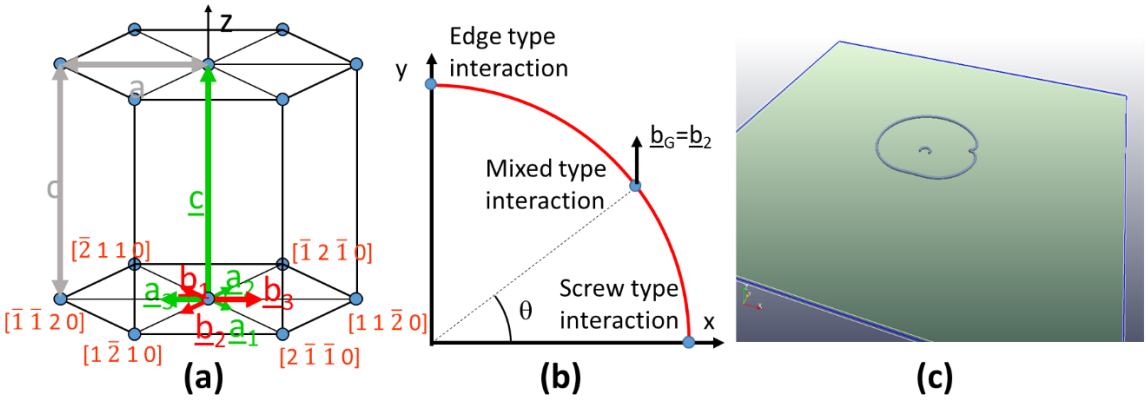

Figure ***1***). The Burgers vector of the dislocation $\underline{b_G} = \underline{b_2} = 1/3[1\bar{2}10]$ is always parallel to the y axis. A constant shear stress equal to σ_{yz} =120 MPa is applied to activate the source. After the closing of the source, the resulting dislocation is circular in the prismatic plane and slightly elliptical in the basal plane. A dislocation segment can be tracked by the polar angle, θ, as shown in

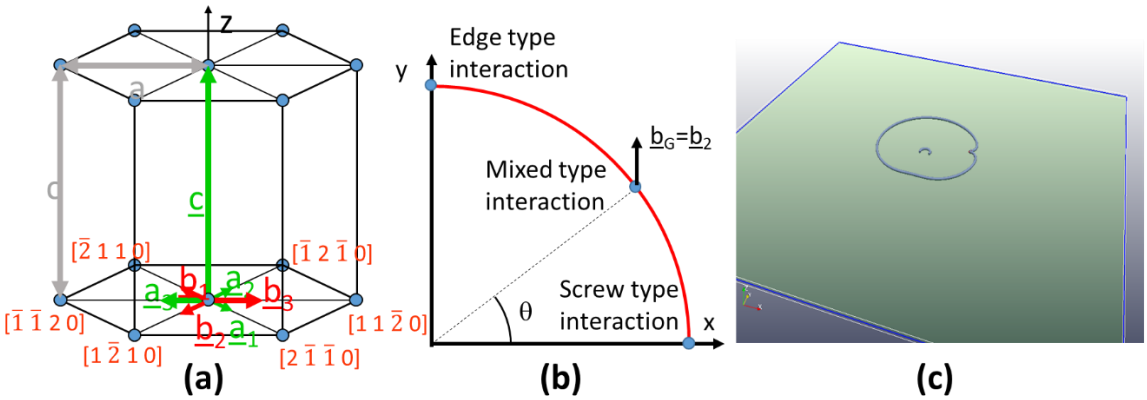

Figure ***1***. The interaction of the dislocation and one loop is then systematically studied starting from the screw type interaction location (θ=0°) to the edge type interaction location (θ=90°), through all the possible mixed type interactions. Furthermore, the Burgers vector of the loop is also systematically changed and can be either $\underline{b_L} = \underline{b_2}$, $\underline{b_L} = \underline{b_1}$ or $\underline{b_L} = \underline{b_3}$. The loop introduced is an interstitial loop in a shape of square with sides of 20 nm long. The ability for the loop, depending on the configuration studied, to pin the dislocation or to be swept away by the dislocation is then analyzed.

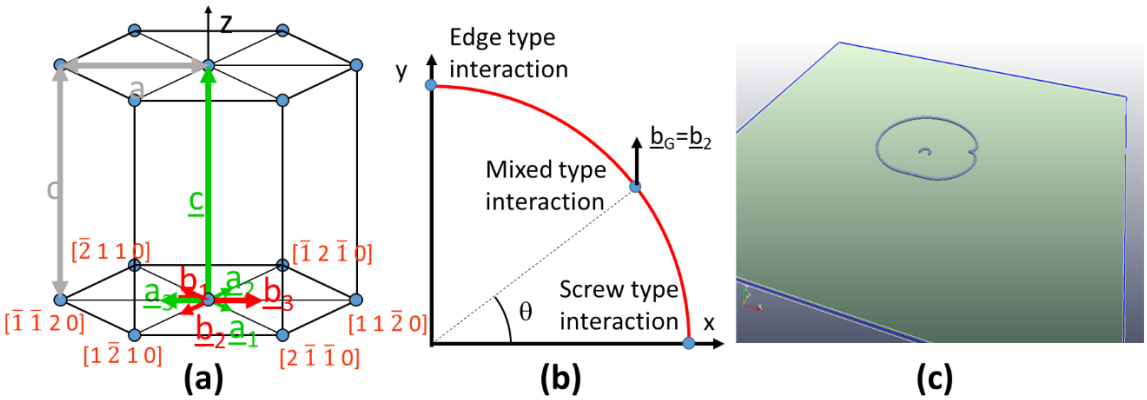

Figure 1 : (a) 4-indices Miller-Bravais convention for HCP structure. (b) Schematic describing the systematic study of interactions between mixed dislocations and loops. (c) Snapshot of the simulation box showing the interaction between a loop and a dislocation with the same Burgers vector (θ=10°).

Finally, several other DD simulations have been performed on geometry representative of the configurations observed during in situ TEM straining experiments. In that case, the two impenetrable upper and lower surfaces of the box account for the TEM thin foil surfaces that are covered by a thin oxide layer. The orientation of the grain analyzed by TEM is introduced into the simulation. A uniaxial tensile loading is applied with a constant applied stress. The other details concerning these simulations will be described further in the following of the article.

3. Study of interactions between loops and mixed dislocations gliding either in the prismatic or basal plane

Following the work described in [17], systematic DD simulations have been performed for dislocations gliding either in the basal or in the prismatic plane and interacting with loops. However, in this previous study, small simulation boxes with periodic boundary conditions along the dislocation line were used. As described above, this induced some artifacts on the resulting interaction. This is why in this new study, DD simulations have not been restricted to pure screw or pure edge dislocations and larger simulation box without periodic boundary conditions have been used.

Starting from the Frank-Read source (

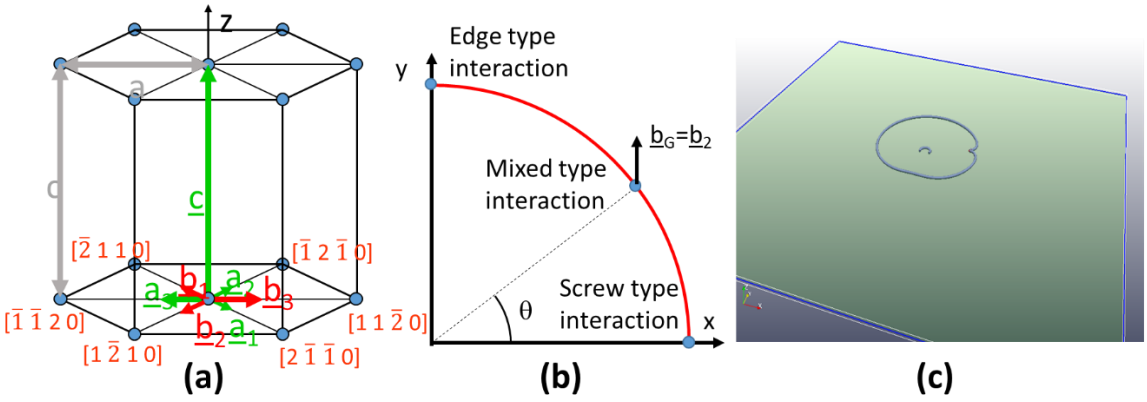

Figure ***1***), various locations for the loop along the dislocation line (every 10°) were tested, each location for the loop being a single computation. It appears that the resulting interaction depends strongly on the location of the loop with respect to the local character of the dislocation, defined by the angle, φ, between the local dislocation segment and the Burgers vector. For the sake of simplicity, the polar angle θ between the x-axis and the loop location, starting from the center of the elliptical dislocation has been used. In the case of a circular dislocation, which is the case for the dislocation source in the prismatic plane, the angle φ and the polar angle θ are equal. The dislocation source in the basal plane is slightly elliptical. This is because of the difference in the Poisson's ratio computed by the Bacon-Scattergood procedure.

The ratio between the half-length of the ellipse along the x-axis (l_x) and the half-length of the ellipse along the y-axis (l_y) is equal to 1.29 for basal dislocations, whereas it is equal to 1.03 for prismatic ones. There is a relationship, given by Equation 5, between the angle φ characterizing the local character of the dislocation and the polar angle θ.

$$\tan(\varphi) = \left(\frac{l_x}{l_y}\right)^2 \tan(\theta) \qquad (5)$$

Firstly, interactions between a loop and a dislocation gliding in the prismatic plane are simulated. The gliding dislocation has a Burgers vector $\underline{b_G} = \underline{b_2}$, parallel to the y-axis. The results of the interaction between the dislocation and interstitial loops with Burgers vector $\underline{b_L} = \underline{b_2}$ are described in the following.

- 0°≤θ≤10°: Strong pinning, no clearing. Formation of a helical turn. Then closing of the helical turn. The loop is left unchanged behind (Figure 2a-d).
- 15°≤θ≤40°: Strong pinning, no clearing. The loop is incorporated into the dislocation line as a helical turn. Then, half of the loop is left behind. Later, the other half is also left behind.
- 45°≤θ≤75°: No pinning and partial clearing. The loop is incorporated into the dislocation as a helical turn. A reaction then occurs leading to the formation of a double

super-jog dragged by the dislocation. Half of the loop is left behind. Partial clearing (Figure 2e-h).

- 80°≤θ≤90°: Weak pinning and partial or no clearing. The loop is incorporated into the dislocation, slightly dragged by the dislocation and eventually left behind unchanged. Depending on the height of the loop with respect to the gliding plane, the loop can also be incorporated as a double super-jog.

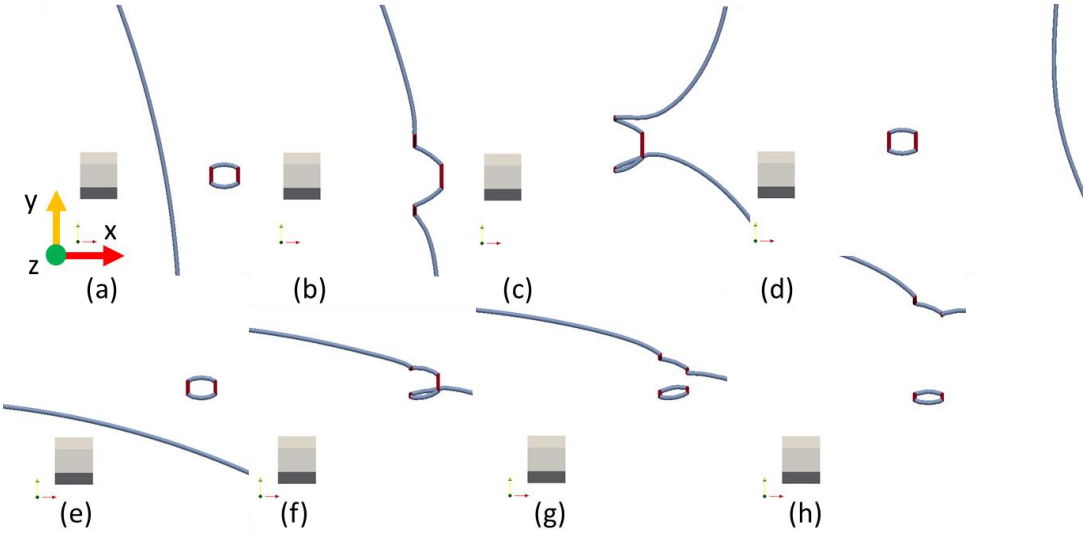

Figure 2 : Sequence showing an interaction between a mixed dislocation of Burgers vector $\underline{b}_G = \underline{b}_2$ gliding in the prismatic plane and a loop with Burgers vector $\underline{b}_L = \underline{b}_2$. (a), (b), (c), (d) θ=10°: strong pinning, no clearing. (e) (f) (g) (h) θ=72°: partial clearing, no pinning.

The results of the interaction between the dislocation ($\underline{b}_G = \underline{b}_2$) and loop ($\underline{b}_L = \underline{b}_1$) are described in the following. Due to the symmetry of the system, the interactions with a loop with Burgers vector $\underline{b}_L = \underline{b}_3$ yield to exactly the same results.

- 0°≤θ≤5°: Strong pinning, no clearing. Formation of a junction. The dislocation fully reacts with the loop and leaves the loop behind with a Burgers vector modified, equal to $\underline{b}_L = \underline{b}_2$.
- 10°≤θ≤30°: Strong pinning, no clearing. Formation of a junction that reacts with the loop creating a helix turn. The helix turn is then closed, pulled on both sides by the gliding dislocation. Then the loop is left behind with a modified Burgers vector $\underline{b}_L = \underline{b}_2$ (Figure 3a-d).
- 35°≤θ≤45°: Medium pinning & limited clearing. Formation of a junction that reacts with the loop creating a double super-jog. The double super-jog is slightly dragged on its cylinder. The double super-jog is then closed, pulled on both sides by the gliding dislocation. Then the loop is left behind with a modified Burgers vector $\underline{b}_L = \underline{b}_2$.

- 50°≤θ≤90°: Weak pinning & full clearing. Formation of a junction. The junction reacts with the loop leading to the full incorporation of the loop as a double super-jog. The double super-jog is dragged by the dislocation leading to a full clearing (Figure 3e-h).

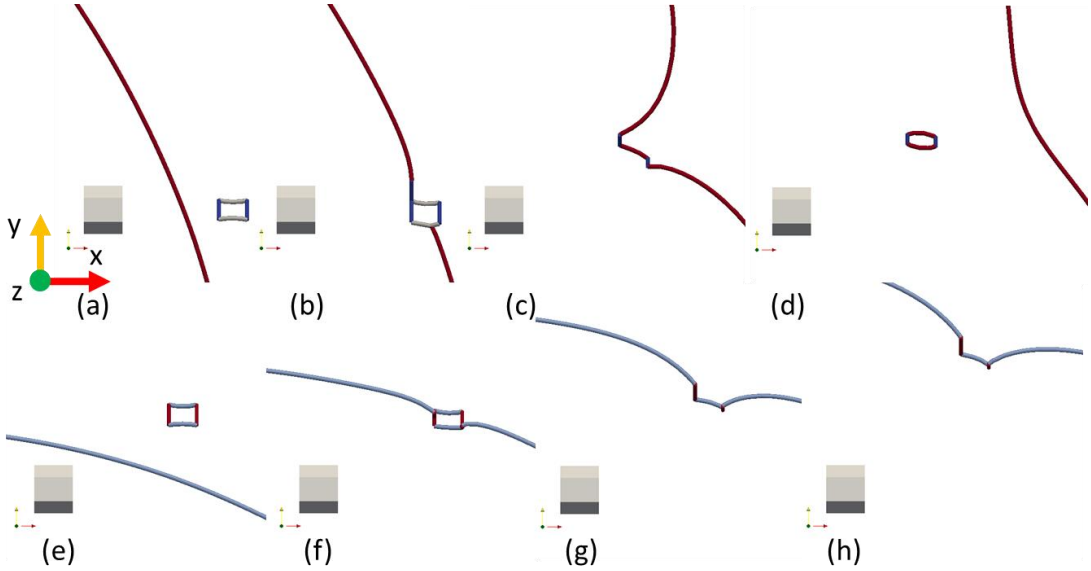

Figure 3 : Sequence showing an interaction between a mixed dislocation of Burgers vector $\underline{b}_G = \underline{b}_2$ gliding in the prismatic plane and a loop with Burgers vector $\underline{b}_L = \underline{b}_1$. (a), (b), (c), (d) θ=21°: strong pinning, no clearing. (e), (f), (g), (h) θ=72°: full clearing, no pinning.

The results of the interactions are summarized schematically on **Figure 4**a-c using a polar plot. In red is shown the angular domain where the interaction leads to strong pinning and no clearing because of the incorporation of the loop into the dislocation as a helical turn. In green is shown the angular domain where the interaction leads to partial or full clearing and no pinning because of the incorporation of the loop into the dislocation as a double super-jog that is dragged on its cylinder. The blue light domain corresponds to the nearly pure edge configuration where the interaction is relatively weak and can lead either to no or partial clearing depending on the height of the loop with respect to the glide plane.

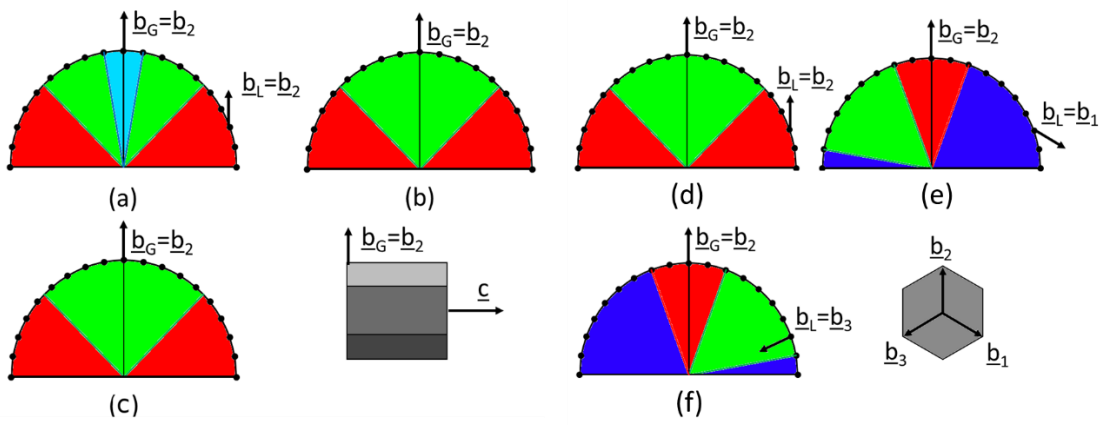

Figure 4 : Results of interactions between loops and a mixed dislocation with Burgers vector $\underline{b}_G = \underline{b}_2$ gliding in (a), (b), (c) the prismatic plane, or in (c), (d), (e) the basal plane. (a) (d) Loop with Burgers vector $\underline{b}_L = \underline{b}_2$. (b) (e) Loop with Burgers vector $\underline{b}_L = \underline{b}_1$. (c) (f) Loop with Burgers vector $\underline{b}_L = \underline{b}_3$. Green: clearing and no pinning. Red: strong pinning and no clearing. Light blue: special configuration with weak pinning and partial or no clearing. Dark blue: no clearing but also no pinning.

These new results appear to be rather consistent compared with previous simulations involving only pure edge and pure screw dislocations [17]. Indeed, for pure edge dislocations, the previous results yield respectively to partial, or full clearing, for $\underline{b}_L = \underline{b}_2$, or $\underline{b}_L = \underline{b}_1$. The "light blue interaction" type was not observed in these early simulations. Concerning pure screw dislocations, the agreement is also good since all interactions yielded to the incorporation of the loop into the dislocation as a helical turn. However, in the small simulation box with periodic boundary conditions used previously, the helical turn expanded leading to the disappearance of the dislocation segments gliding in the prismatic plane. This is not the case for these new simulations.

Because in the material, <a> loops with the three different Burgers vectors can be found in the same proportion, when one prismatic slip system, with one Burgers vector ($\underline{b}_G = \underline{b}_2$), is activated, all these interactions can be found to occur at the same time. One third of interactions will be of the type $\underline{b}_L = \underline{b}_G = \underline{b}_2$ (**Figure 4**a) and two third of interactions will be of the type $\underline{b}_L = \underline{b}_1$ (**Figure 4**b). As illustrated on **Figure 4**, partial or full clearing occurs only close to the edge direction, up to 45° to the edge direction. Along the screw direction, a strong pinning occurs in every case, and no clearing occurs. This leads to a very difficult expansion of dislocation source in the prismatic planes. This explains the significant hardening of the prismatic slip after irradiation. Furthermore, the clearing process can only proceed along the edge direction of the dislocation source, again resulting in a limited and difficult channeling process in the prismatic plane.

In a second step, interactions between a loop and a dislocation gliding in the basal plane are simulated. For dislocations gliding in the basal plane, the same parameters for the dislocation energy per unit length, as the one deduced for prismatic slip are used.

The results of the interaction between the dislocation and loops with Burgers vector $\underline{b_L} = \underline{b_2}$ are described in the following.

- 0°≤θ≤15°: Strong pinning, no clearing. Formation of a helical turn. Then closing of the helical turn. The loop is left unchanged behind (**Figure 5**a-d).
- 20°≤θ≤40°: Strong pinning, no clearing. The loop is incorporated into the dislocation line as a helical turn. The helical turn is slightly dragged on its cylinder. Then half of the loop is left behind. Later the other half is also left behind. For θ=40° the full loop is left behind.
- 45°≤θ≤90°: No pinning & partial clearing. The loop is incorporated into the dislocation as a helical turn. A reaction then occurs leading to the formation of a double super-jog dragged by the dislocation. Half of the loop is left behind. Partial clearing (**Figure 5**e-h).

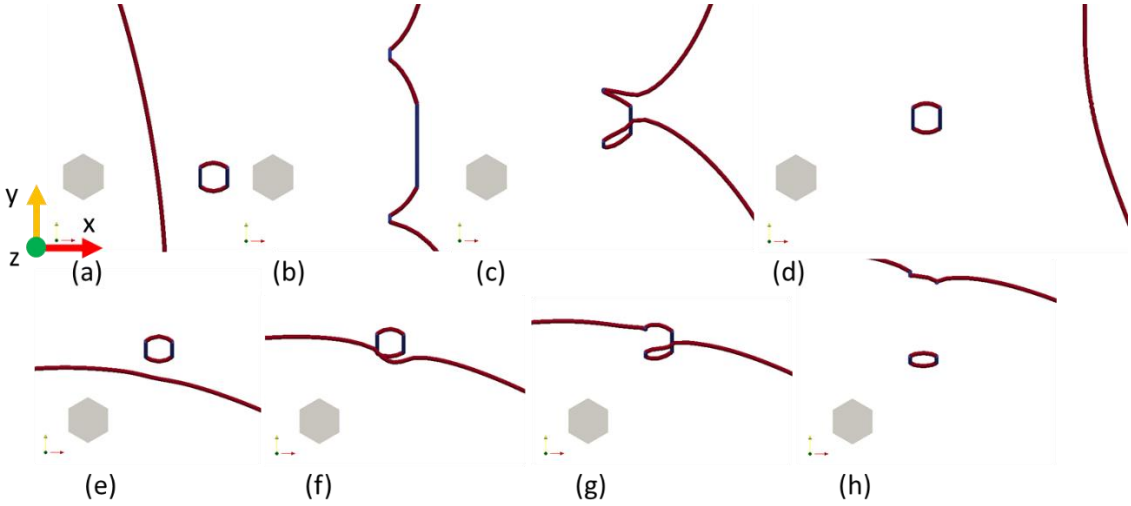

Figure 5 : Sequence showing an interaction between a mixed dislocation of Burgers vector $\underline{b_G} = \underline{b_2}$ gliding in the basal plane and a loop with Burgers vector $\underline{b_L} = \underline{b_2}$. (a), (b) (c) (d) θ=10°: strong pinning, no clearing. (e) (f) (g) (h) θ=84°: partial clearing, no pinning.

The results of the interaction between the dislocation ($\underline{b_G} = \underline{b_2}$) and loops with Burgers vector $\underline{b_L} = \underline{b_1}$ are described in the following.

- 0°≤θ≤20°: No pinning, no clearing. Formation of a crossed-state. Very weak interaction. The loop is slightly pushed aside, gliding on its cylinder. Then the loop is left unchanged.

- 25°≤θ≤65°: No pinning, no clearing. Formation of a junction, glissile in the basal plane. The loop is slightly pushed aside on its cylinder. Then the dislocation easily overcomes the loop leaving the loop unchanged (**Figure *6***a-d).
- 70°≤θ≤90°: Strong pinning, no clearing. Formation of a junction. The loop does not move. The dislocation overcomes the loop after significant pinning, leaving the loop unchanged (**Figure *6***e-h).

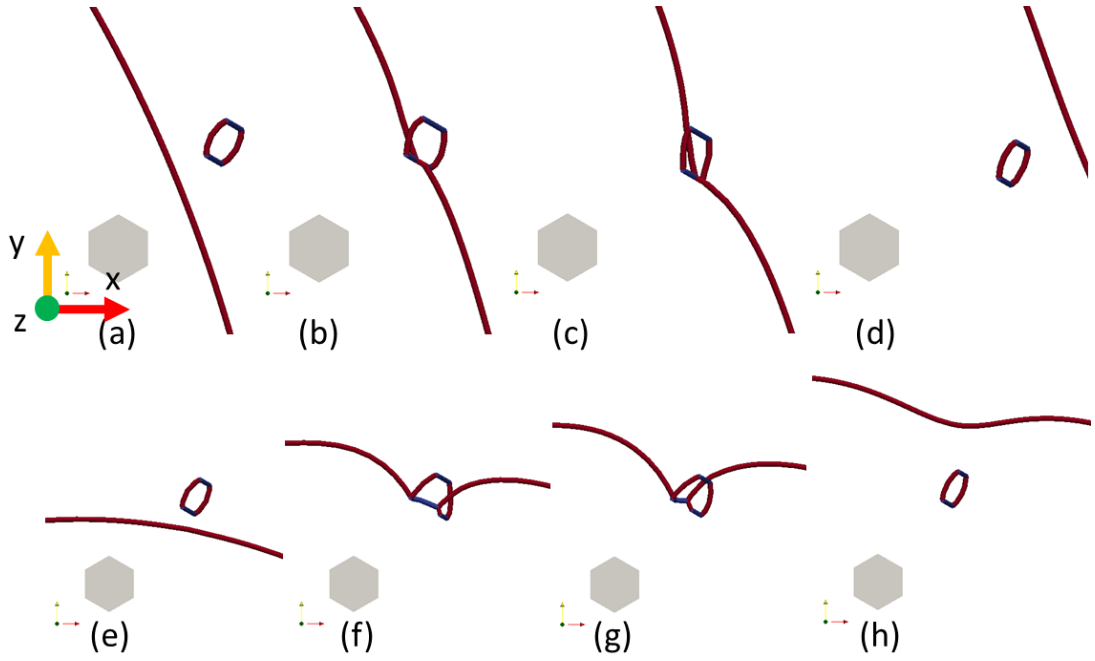

Figure 6 : Sequence showing an interaction between a mixed dislocation of Burgers vector $\underline{b}_G = \underline{b}_2$ gliding in the basal plane and a loop with Burgers vector $\underline{b}_L = \underline{b}_1$. (a), (b), (c) (d) θ=32°: no pinning, no clearing. (e), (f), (g), (h) θ=84°: strong pinning, no clearing.

In the case of basal slip, contrary to prismatic slip, the system is not anymore symmetric. Simulations with $\underline{b}_L = \underline{b}_3$ are then also described in the following.

- 0°≤θ≤10°: No pinning, no clearing. Formation of a crossed-state. Very weak interaction. The loop is slightly pushed aside, gliding on its cylinder. Then the loop is left unchanged.
- 15°≤θ≤65°: No pinning, significant clearing. Formation of a crossed-state or a junction, glissile in the basal plane. The loop is pushed aside on its cylinder over a long distance. Eventually the loop is left unchanged after significant clearing. For θ= 54° the loop is dragged during the full simulation duration (**Figure 7**a-d).
- 70°≤θ≤90°: Strong pinning, limited clearing. Formation of a junction. The loop is slightly pushed on its cylinder. The dislocation overcomes the loop after a strong pinning, leaving the loop unchanged (**Figure 7**e-h).

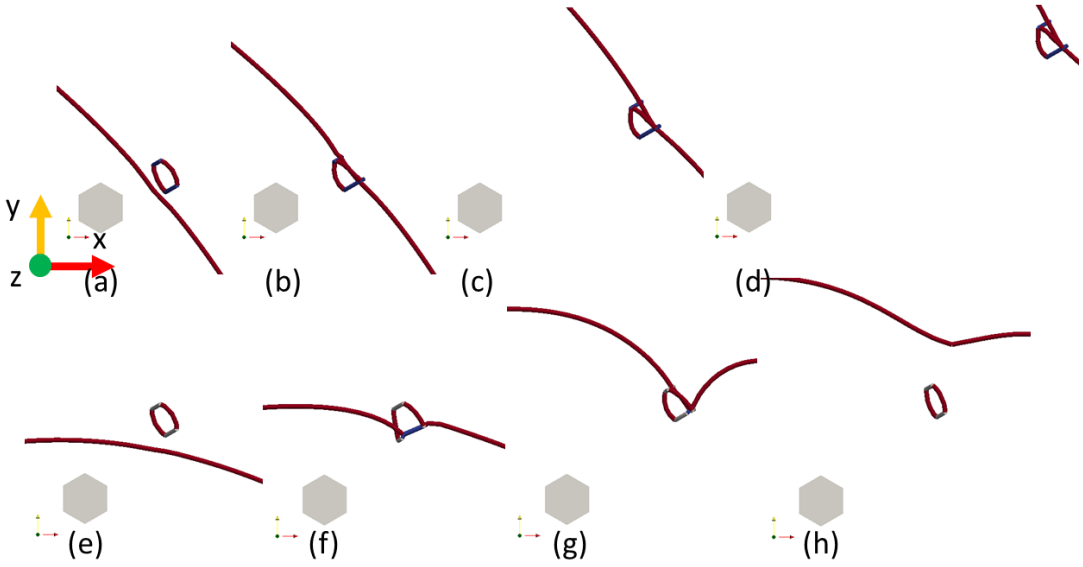

Figure 7 : Sequence showing an interaction between a mixed dislocation of Burgers vector $\underline{b}_G = \underline{b}_2$ gliding in the basal plane and a loop with Burgers vector $\underline{b}_L = \underline{b}_3$. (a), (b), (c), (d) θ=54°: no pinning, significant clearing. (e) (f) (g) (h) θ=84°: strong pinning, no clearing.

The results of the interactions are also summarized on **Figure 4**d-f. In this plot, the dark blue domain corresponds to the case when the interaction between the dislocation and the loop is very weak (no pinning) but the loop is not cleared by the dislocation.

Again, these results are consistent with previous simulations involving only pure edge and pure screw dislocations [17]. For pure screw dislocation with a different Burgers vector than that of the loop, we also obtained, in early simulations, the formation of a crossed-state that was assumed to allow the clearing of loops. These new simulations bring a renewed light on the role of the orientation of the loop glide cylinder with respect to the character of the dislocation. Indeed, clearing only occurs, for dislocation and loop with different Burgers vector ($\underline{b}_G = \underline{b}_2$ and $\underline{b}_L = \underline{b}_3$), for the polar angle (θ) between 15° up to 65° **Figure 4**f. This angular domain is around the glide cylinder of the loop, orientated at 30° with respect to the x-direction. Because the dislocation is not circular in the basal plane, the maximum clearing does not occur for a polar angle of 30°, but for a higher polar angle. The local normal direction of the dislocation (velocity vector) makes an angle of φ=30° for a polar angle equals to θ=43°. This position should then be the best orientation for the glide of the loop along its cylinder. The best orientation for the glide of the loop on its cylinder is θ=54°. This may be explained by the fact that as the ellipse expands, the loop is dragged on its cylinder along its Burgers vector ($\underline{b}_L = \underline{b}_3$), leading to the progressive decrease of the angle θ. This in turn results in a decrease of the φ angle that can eventually lead to the release of the loop. This is probably why starting with a higher θ can lead to a delayed release of the loop.

Furthermore, it is worth noticing that for the other configurations involving dislocation and loop with different Burgers vector ($\underline{b}_G = \underline{b}_2$ and $\underline{b}_L = \underline{b}_1$), the interaction between the dislocation and the loop is very weak for a polar angle between 0° up to 65° (**Figure 4**e) Although there is no clearing for this configuration, there is also no pinning. This allows the dislocation to glide easily through loops for this entire angular domain.

Of course, as for prismatic slip, the dislocation gliding in the basal plane encounters the three types of loops. The resulting interaction is therefore a mix between all these interactions. One type of loop (one third, with Burgers vector $\underline{b}_2$) will be partially cleared close to the edge direction. The loops with Burgers vector $\underline{b}_3$ (one third) will be either fully or partially cleared, in the angular domain between 15° and 65°. Finally, the loops with Burgers vector $\underline{b}_1$ (one third) will be fully, or partially, cleared in the angular domain between 115° and 165°. In addition, the dislocation will be able to glide in this angular domain rather easily, being only pinned by one type of loops ($\underline{b}_2$). This thus explains that, in the presence of loops, the glide of dislocations in the basal plane is easier than the glide of the prismatic plane, because of less pinning. It also explains that the clearing of loops in the basal plane is easier than in the prismatic plane.

Another major difference between prismatic and basal glide, which can contribute to the formation of defect free channels in irradiated zirconium alloys, is the fact that if the three different basal slip systems (different Burgers vectors) are activated at the same time in close parallel planes, then all the loops can be easily cleared away.

4. Experimental results and comparison with numerical simulations

In order to bring experimental proof concerning dislocation and loop interactions, in situ straining experiments have been conducted in a TEM on recrystallized Zircaloy-4 irradiated at 450°C with Zr ions. After irradiation, large interstitial <a> loops were observed. Furthermore, because of alloying elements present in Zircaloy-4, the effect of ion irradiation may not be only to create dislocation loops. This could play some role on the deformation mechanisms as compared to pure zirconium.

Several interactions between dislocations and loops have been observed. Two interactions, representative of the two main phenomena observed are reported here. The first interaction (Figure 8) shows the strong pinning of a dislocation by a loop. The dislocation glides in the first order pyramidal plane at 400°C. Then the dislocation overcomes the loop. The second interaction obtained at 350°C (Figure 9) shows the incorporation of a loop into the dislocation, also gliding in the first order pyramidal plane. The loop is first incorporated on the edge side of the dislocation, creating a double super-jog and then it moves to the screw side of the dislocation and becomes a helical turn.

Following the approach described in [19], these two configurations have been simulated by DD owing to the introduction of experimental inputs. First, the orientation of the grain has been determined by electron diffraction. The analysis of the slip traces observed on the two

foil surfaces indicate that, in the two cases, the dislocations glide in a first order pyramidal plane. The size of the loop was evaluated directly from the image. The loop nature was taken as interstitial since after Zr ion irradiation mostly interstitial loops have been observed [20]. Because the position of the loop in the foil thickness, with respect to the glide plane of the dislocation, is unknown, various positions are then tested to obtain the best agreement between simulation and experiment. Furthermore, the shear stress moving the dislocation was estimated from its curvature, knowing its Burgers vector and its glide plane [26, 27].

As explained earlier, several materials dependent parameters must be chosen to simulate the behavior of <a> dislocations gliding in pyramidal plane in Zircaloy-4 at these temperatures. The anisotropic elastic coefficients for temperatures of 350°C and 400°C can be found in [28]. Isotropic elastic coefficients have been deduced using Voigt's procedure described in [29], yielding μ=29.2 GPa and ν=0.36. These coefficients leads to a Young's modulus of 79 GPa, which is in correct agreement with experimental values measured at these temperatures [30, 31]. Concerning the dislocation energy parameters, they have been chosen equal to the one used in a previous work [19], that is a_0=3.23 Å and E_{core}^0=0.052 eV/Å.

4.1. Experimental case #1 : pinning of the dislocation by the loop

In a previous study, the friction coefficient was evaluated as being equal to 3×10^5 Pa.s for <a> pyramidal slip [19]. This value has also been used to start with. However, when conducting the simulations, it appeared that the loop was a much stronger obstacle than expected based on the previous simulations. The friction coefficients for the other slip systems (basal and prismatic) were increased ($B_P = 3\times10^6$ Pa.s; $B_{\pi a}$=3×10^5 Pa.s; B_B = 3×10^7 Pa.s), leading to the locking of the loop. The additional friction due to the constricted nodes is not taken into account here. For this simulation, a uniaxial tensile stress is applied along the y-direction. The magnitude of the tensile stress is σ_{yy}=158 MPa, accordingly to the evaluation based on the curvature of the dislocation.

It can be noticed on **Figure *8*** that, with these parameters, both the kinetics and the geometry of the interaction are satisfactory reproduced. From these simulations, we can learn that this loop acts as a stronger pinning point than expected probably because of solute atoms, such as oxygen, have diffused to the loop creating a solute atmosphere that can lock the loop motion. We can also learn that the loop has probably the same Burgers vector as the dislocation, since this configuration was the one that lead to the best agreement, compared to other trials.

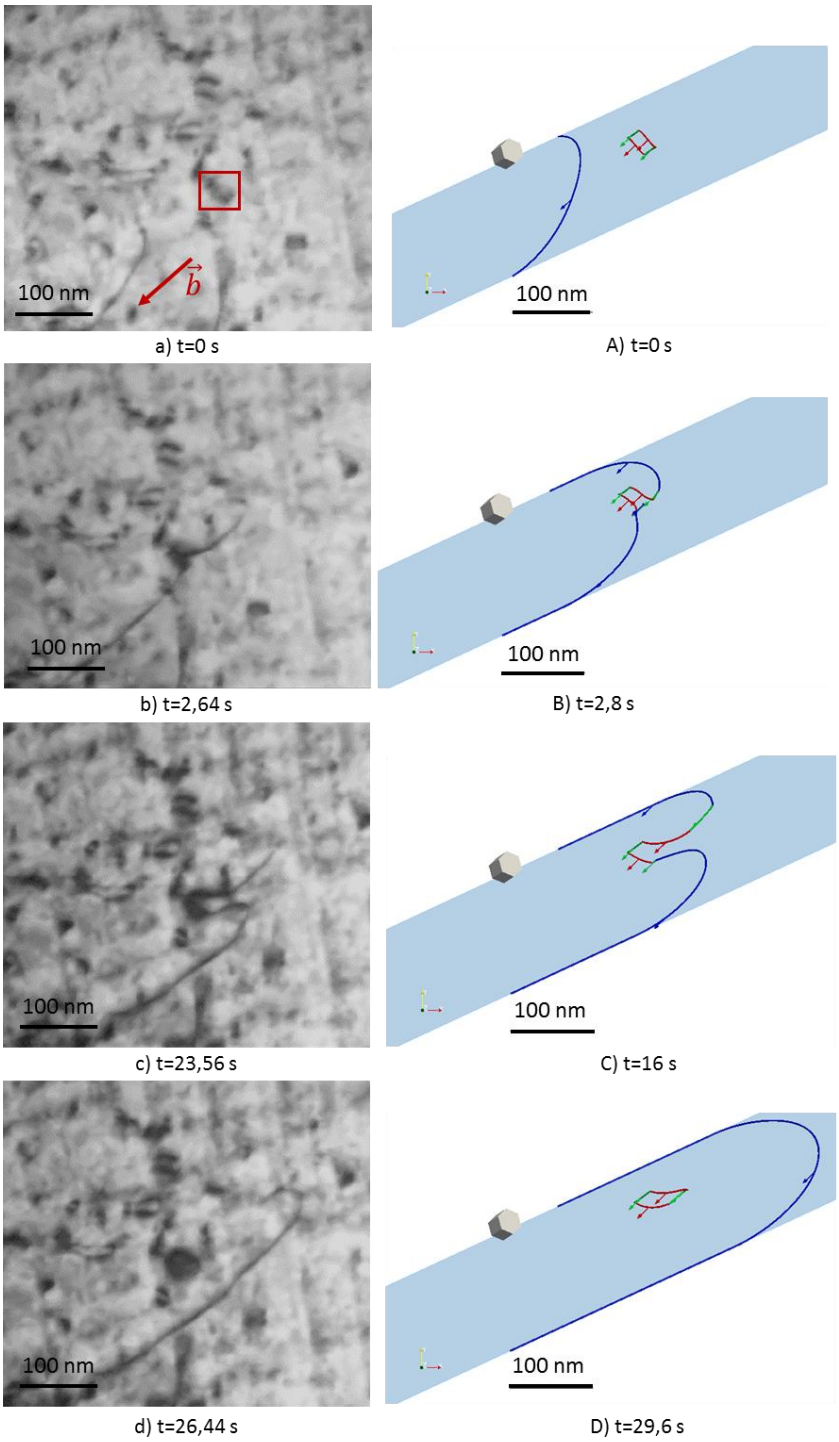

Figure 8 : Pinning case. a) to d) In situ observation in a TEM of a dislocation interacting with a loop. A) to D) DD simulation of the dislocation – loop interaction.

4.2. Experimental case #2 : incorporation of the loop as helical turn

Starting with the same parameters set we tried to simulate a second interaction. From the curvature of the dislocation, the applied stress was estimated as σ_{yy}=124 MPa considering a uniaxial applied stress along the y-direction. However, the dislocation velocity was very low in

this experiment. The reason for this very low velocity was not clearly understood. This may be explained by an overestimated applied stress because of a curvature that is not due to the stress but to a motion mechanism involving kink pair to overcome strong Peierls valleys, as it was observed previously for <a>-pyramidal slip [32]. In order to account for this very low dislocation velocity, the friction for the pyramidal plane was artificially increased. The other friction coefficients were also modified in order to obtain the best possible agreement B_P=1×10^6 Pa.s; $B_{\pi a}$= 3×10^6 Pa.s ; B_B= 1×10^7 Pa.s.

It can be seen on **Figure *9*** that with this parameter set, the agreement between the simulation and the experiment is correct, although from the timescale point of view there are still significant discrepancies. From these simulations, we can learn that the loop has probably not the same Burgers vector as the dislocation. The loop is incorporated as a double super-jog into the dislocation, on the edge side. Then the loop is pushed aside, on the screw part leading to the formation of a helical turn. In the simulation, we have also introduced a second loop, which is difficult to see clearly on the film. This second loop also explains the wavy shape of the dislocation.

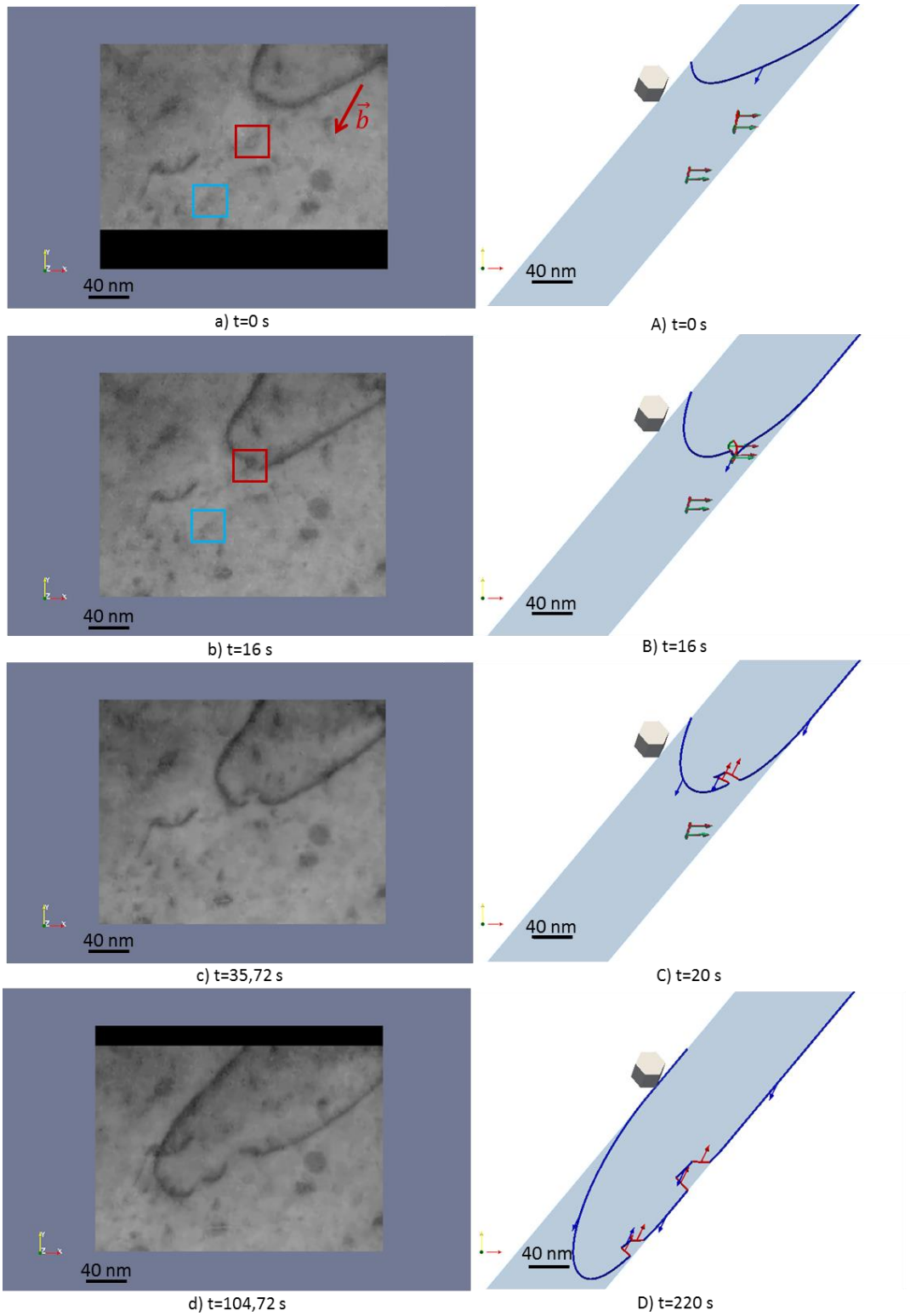

Figure 9 : Incorporation case. a) to d) In situ observation in a TEM of a dislocation interacting with a loop. A) to D) DD simulation of the dislocation – loop interaction.

6. Discussion

From the systematic study of interactions between dislocations and loops using DD simulations adjusted on MD simulations, we have been able to bring a new light on the deformation mechanisms occurring in neutron-irradiated zirconium alloys. Indeed, the origin of the easier basal glide, and basal loop clearing, observed by TEM after irradiation [8,11,12,13], is now better understood. It is clearly due to the weak interactions between dislocation and loops in the screw-mixed direction (for loops with different Burgers vector than the dislocation) and to the easy clearing of loops along their glide cylinder which is along the mixed direction. On the contrary, dislocations gliding in the prismatic planes are always strongly pinned in the screw-mixed direction. The dislocation source is thus very strongly constrained for prismatic slip resulting in a high flow stress. On the other hand, the dislocation source in the basal plane is able to expand along the screw-mixed direction leading to a lower flow stress needed to activate the dislocation source. Another reason for the easier clearing of loops by basal glide is the fact that the three <a> Burgers vectors all belong to the basal plane. If three dislocation sources, with different <a> Burgers vectors are activated in close parallel basal planes, they should be able to clear out all the loops leading to the formation of a dislocation channel.

To be able to reproduce in situ straining experiments done on Zircaloy-4 using DD simulations, the friction coefficient (here for pyramidal <a> slip) must be increased by a factor 10^{10} compared to the friction coefficient measured for prismatic slip by MD simulations. This is very surprising and can be partly attributed to the fact that first order pyramidal slip with <a> Burgers vector is more difficult to activate than the prismatic slip and has therefore a higher friction coefficient compared to the prismatic slip.

This discrepancy may also be attributed to the non-linearity of the visco-plastic flow law (Eq. 1). Indeed, the linearization of the non-linear flow low at very high shear strain rate, as it is the case in MD simulations, yields very low friction coefficient (B) whereas for the very low shear strain rate used in the experiments, the linearization of the flow law leads to a very high friction coefficient.

Lastly, this discrepancy has been attributed [19] to the effect of solute atoms such as oxygen that may strongly affect the dislocation motion. Indeed, it has been recently established, using ab initio calculations [33], that oxygen atoms induce a local cross-slip of a screw dislocation, initially gliding in the prismatic plane, leading to the formation of jogs that have to be dragged by the dislocation during its glide in the prismatic plane. This explains the hardening effect of oxygen atoms. Furthermore, at specific temperatures, a dynamic strain-aging phenomenon also occurs with oxygen atoms, that may increase the hardening effect. This last issue should thus be investigated in more detail to extend the conclusions, obtained on pure zirconium, to zirconium alloys.

6. Conclusion

A multi-scale numerical study has been conducted to investigate interactions between dislocations and radiation induced loops in zirconium. Complex configurations involving mixed curved dislocations interacting with loops have been simulated using a dislocation dynamics. The input parameters were adjusted on molecular dynamics simulations. We have brought a clear picture of the reason why dislocation glide and clearing of loops in the basal plane is easier than in the prismatic plane after irradiation, as shown by experiments. Indeed, in the mixed-screw directions, dislocations in the prismatic plane are always strongly pinned whereas in the basal plane, for some configurations, clearing of loops or weak interactions occur, allowing clearing and easy glide in this plane. Furthermore, all three basal systems can contribute to clearing in the basal plane contrary to prismatic slip. These two reasons explain the easy basal glide and clearing of loops after irradiation.

Moreover, *in-situ* straining experiments inside a TEM, conducted on ion irradiated zirconium alloy samples show interactions between dislocations and loops. The dislocation dynamics simulations are able to reproduce the TEM observations, after adjustment of some parameters, showing the relevance of this numerical tool. Some experiments also suggest that solute atoms, such as oxygen, could play a role on the pinning of some loops. More studies are probably needed to assess this last point.

In a future prospect, massive dislocation dynamics simulations, involving many loops and many dislocations, could now be used with confidence to simulate the formation of defect free channels in irradiated zirconium. This will eventually give access to a fully predictive constitutive law, at the grain scale, allowing the prediction of the mechanical behavior of zirconium alloys after neutron irradiation.

Acknowledgements

The authors thank EDF and Framatome for supporting this study.

References

[1] Onimus, F., Béchade, J.L. (2012). Radiation effects in zirconium alloys. Comprehensive Nuclear Materials, Vol. 4, edited by R. J. M. Konings, pp. 1–31. Amsterdam: Elsevier.

[2] Griffiths, M. (1988). A review of microstructure evolution in zirconium alloys during irradiation. Journal of Nuclear Materials, 159, 190-218.

[3] Coleman, C. E., Mills, D., & Van der Kuur, J. (1972). Deformation parameters of neutron irradiated Zircaloy-4 at 300 C. Canadian Metallurgical Quarterly, 11(1), 91-100.

[4] Onchi, T., Kayano, H., & Higashiguchi, Y. (1980). The inhomogeneous deformation behaviour of neutron irradiated Zircaloy-2. Journal of Nuclear Materials, 88(2-3), 226-235.

[5] R. Adamson and W. Bell, “Effects of neutron irradiation and oxygen content on the microstructure and mechanical properties of Zircaloy,” in Microstructure and Mechanical Behaviour of Materials., Xian, China, 1985, vol. 1, pp. 237–246.

[6] R. Adamson, S. Wisner, R. Tucker, and R. Rand, “Failure Strain for Irradiated Zircaloy Based on Subsized Specimen Testing and Analysis,” Use Small-Scale Specim. Test. Irradiat. Mater., vol. ASTM STP 888, pp. 171–184, 1986.

[7] K. Petterson, “Evidence for basal or near-basal slip in irradiated Zircaloy,” J. Nucl. Mater., vol. 105, pp. 341–344, 1982.

[8] Fregonese, M., Régnard, C., Rouillon, L., Magnin, T., Lefebvre, F., & Lemaignan, C. (2000, January). Failure Mechanisms of irradiated Zr alloys related to PCI: Activated slip systems, localized strains, and iodine-induced stress corrosion cracking. In Zirconium in the Nuclear Industry: Twelfth International Symposium. ASTM International.

[9] Farrell, K., Byun, T. S., & Hashimoto, N. (2004). Deformation mode maps for tensile deformation of neutron-irradiated structural alloys. Journal of nuclear materials, 335(3), 471-486.

[10] Onimus, F., Monnet, I., Béchade, J. L., Prioul, C., Pilvin, P. (2004). A statistical TEM investigation of dislocation channeling mechanism in neutron irradiated zirconium alloys. Journal of Nuclear Materials, 328(2-3), 165-179.

[11] Onimus, F., Béchade, J., Prioul, C., Pilvin, P., Monnet, I., Doriot, S., Mardon, J. (2005, September). Plastic deformation of irradiated zirconium alloys: TEM investigations and micro–mechanical modelling. In 14th International Symposium on Zirconium in the Nuclear Industry, ASTM STP (Vol. 1467, pp. 53-77).

[12] Bourdiliau, B., Onimus, F., Cappelaere, C., Pivetaud, V., Bouffioux, P., Chabretou, V., Miquet, A. (2012, April). Impact of irradiation damage recovery during transportation on the subsequent room temperature tensile behavior of irradiated zirconium alloys. In Zirconium in the Nuclear Industry: 16th International Symposium. ASTM International.

[13] Onimus, F., Béchade, J.L., Gilbon, D. (2013). Experimental analysis of slip systems activation in neutron-irradiated zirconium alloys and comparison with polycrystalline model simulations. Metallurgical and Materials Transactions A, 44(1), 45-60.

[14] R. E. Voskoboynikov, Y. N. Osetsky, and D. J. Bacon, “Self-interstitial atom clusters as obstacles to glide of edge dislocations in α-zirconium,” Mater. Sci. Eng. A, vol. 400–401, pp. 54–58, Jul. 2005.

[15] Serra, A., Bacon, D.J. (2013). Atomic-level computer simulation of the interaction between 1/3<11-20>{11-10} dislocations and 1/3<11-20> interstitial loops in α-zirconium. Modelling and Simulation in Materials Science and Engineering, 21(4):045007.

[16] K. Ghavam and R. Gracie, “Simulations of reactions between irradiation induced〈a〉-loops and mixed dislocation lines in zirconium,” J. Nucl. Mater., vol. 462, pp. 126–134, Jul. 2015.

[17] Drouet, J., Dupuy, L., Onimus, F., Mompiou, F., Perusin, S., Ambard, A. (2014). Dislocation dynamics simulations of interactions between gliding dislocations and radiation induced prismatic loops in zirconium. Journal of Nuclear Materials, 449(1-3), 252-262.

[18] Onimus, F., Dupuy, L., Mompiou, F. (2012). In situ TEM observation of interactions between gliding dislocations and prismatic loops in Zr-ion irradiated zirconium alloys. Progress in Nuclear Energy, 57, 77-85.

[19] Drouet, J., Dupuy, L., Onimus, F., Mompiou, F. (2016). A direct comparison between in-situ transmission electron microscopy observations and Dislocation Dynamics simulations of interaction between dislocation and irradiation induced loop in a zirconium alloy. Scripta Materialia, 119, 71-75.

[20] Gaumé, M., Onimus, F., Dupuy, L., Tissot, O., Bachelet, C., Mompiou, F. (2017). Microstructure evolution of recrystallized Zircaloy-4 under charged particles irradiation. Journal of Nuclear Materials, 495, 516-528.

[21] Plimpton, S. (1995). Fast Parallel Algorithms for Short-Range Molecular Dynamics. Journal of Computational Physics, 117(1):1–19.

[22] Kassem, W., Dupuy, L., Onimus, F. (2020). Atomic scale informed Dislocation Dynamics computations. Application to the simulation of interactions between dislocation and radiation induced loops in zirconium. To be published.

[23] Cai, W., Arsenlis, A., Weinberger, C., Bulatov, V. (2006). A non-singular continuum theory of dislocations. Journal of the Mechanics and Physics of Solids, 54(3):561–587.

[24] Scattergood, R.O., Bacon, D. J. (1975). The Orowan mechanism in anisotropic crystals. Philosophical Magazine, 31(1):179–198.

[25] Rodney, D., Martin, G. (2000). Dislocation pinning by glissile interstitial loops in a nickel crystal: A molecular-dynamics study. Physical Review B, 61(13):8714–8725.

[26] Douin, J., Veyssière, P., Beauchamp, P. (1986). Philos. Mag. 54, 375–393.

[27] Caillard, D., Rautenberg, M., Feaugas, X. (2015). Acta Mater. 87, 283–292.

[28] Fisher, E.S., Renken, C.J. (1964). Single-Crystal Elastic Moduli and the hcp bcc Transformation in Ti, Zr, and Hf. Physical Review, 135(2A):A482–A494.

[29] Li., Y., Thompson, R.B. (1990). Relations between elastic constants Cij and texture parameters for hexagonal materials. J. Appl. Phys. 67, 2663.

[30] Schwenk, E.B., Wheeler, K.R. Shearer, G.D., Webster, R.T. (1978). J. Nucl. Mater. 73 129–131.

[31] Northwood, D.O., Rosinger, H.E. (1980). J. Nucl. Mater. 89 147–154.

[32] Caillard, D., Gaumé, M., Onimus, F. (2018). Glide and cross-slip of a-dislocations in Zr and Ti. Acta Materialia, 155, 23-34.

[33] Chaari, N., Rodney, D., Clouet, E. (2017). Oxygen-Dislocation interaction in zirconium from first principles. Acta Materialia, 132, 416-424.